Available online at www.sciencedirect.com

ScienceDirect

Proceedings of the Combustion Institute 36 (2017) 2585–2594

Proceedings of the Combustion Institute

www.elsevier.com/locate/proci

Combustion characteristics of primary reference fuel (PRF) droplets: Single stage high temperature combustion to multistage "Cool Flame" behavior

T.I. Farouk [a,*], Y. Xu [b], C.T. Avedisian [b], F.L. Dryer [c]

[a] Department of Mechanical Engineering, University of South Carolina, Columbia, SC 29208, USA
[b] Sibley School of Mechanical and Aerospace Engineering, Cornell University, Ithaca, NY 14853, USA
[c] Department of Mechanical and Aerospace Engineering, Princeton University, Princeton, NJ 08544, USA

Received 4 December 2015; accepted 15 July 2016
Available online 2 August 2016

Abstract

We report experiments and detailed numerical modeling of mixtures of primary reference fuel (PRF) droplets consisting of *n*-heptane and *iso*-octane with initial droplet diameters of 0.5 and 3.51 mm. The results show a quasi-steady, low temperature (or "Cool Flame" (*CF*)) droplet burning mode that stems from a varying two-stage chemical kinetic behavior of the combustion chemistry. The simulations further illustrate, that the *CF* droplet burning mode in 1 atm air is dependent upon the *iso*-octane fraction and droplet size. *CF* droplet burning is predicted to be absent for large diameter droplets containing more than 50% (by volume) *iso*-octane (>PRF50), and for all droplet diameters that exhibit hot flame burning without radiative extinction. The model predictions are in agreement with new, large diameter PRF50 experiments reported here, as well as previous ground-based PRF50 sub-millimeter diameter experiments. The effects of PRF mixture fraction are further analyzed numerically. Additional simulations show that replacing small amounts of inert (nitrogen) with ozone can sufficiently modify the low temperature kinetic activity of PRF50 droplets to promote *CF* droplet burning, even for sub-millimeter droplet diameters (with no hot flame transition). The implications are that with proper experimental configurations, *CF* droplet burning might be studied in ground-based, sub-millimeter diameter, isolated droplet burning experiments.

Keywords: Primary reference fuel; Cool flame; Droplet combustion; Dual-stage; Bi-component

1. Introduction

Long-duration, "Cool Flame" (*CF*) droplet burning for large diameter, isolated droplets in air (at 1 atm pressure) has been observed aboard the International Space Station (ISS) for *n*-heptane, *n*-octane, and *n*-decane [1–4]. At sufficiently large initial diameters (D_o), the initially transient and high temperature droplet burning process is observed to radiatively extinguish after which a period of *CF* droplet burning ensues that is terminated by diffusive extinction. Detailed numerical analyses for *n*-heptane [3] indicate that the

* Corresponding author. Fax: +1 803 7770106.
E-mail address: tfarouk@sc.edu (T.I. Farouk).

http://dx.doi.org/10.1016/j.proci.2016.07.066
1540-7489

second stage – *CF* burning regime – is closely related to the well-known negative temperature coefficient (NTC) oxidative behavior commonly observed with large carbon number *n*-alkanes [5]. *CF* droplet burning results from a dynamic balance of heat generation from NTC chemical kinetic oxidation and principally diffusive heat loss to the surroundings. Experiments and numerical analyses at higher pressures display dynamic interactions that result in unsteady oscillatory *CF* droplet burning phenomena [6].

Though *CF* droplet burning is different in principle from classical premixed *CF* [1] or two-stage autoignition [5], the existence of low temperature, NTC, and hot ignition kinetic regimes and their dependence on fuel structure, pressure, equivalence ratio, and reaction temperature are key to all of these phenomena. It is well known that the kinetic interactions of other fuel structures with *n*-alkanes can significantly influence the relative importance of these various kinetic regimes and thus, cool flame and autoignition behaviors. For example, mixtures of *n*-heptane and *iso*-octane (2,2,4-trimethylpentane) – Primary Reference Fuel (PRF) mixtures – are often used to generate Motored and Research Octane reference indicators for characterizing two-stage autoignition of gasoline. Despite the large literature on the effects of fuel mixtures on premixed cool flames, autoignition phenomena, and even isolated droplet burning [7], there have been no investigations of how such mixtures might affect *CF* droplet burning behavior.

PRF droplet combustion experiments onboard the ISS were initially motivated to provide additional fundamental observations of mixture composition effects on high temperature combustion properties. However, in conducting these experiments, *CF* droplet burning phenomena were again noted for large diameter experiments undergoing radiative extinction.

In this paper, we report experimental observations from the **Fl**ame **Ex**tinguishment (FLEX) on the ISS for PRF50 mixtures and compare the results with a detailed numerical model (DNM) of the droplet burning process. Both the large diameter droplet observations on ISS and similar sub-millimeter size droplet studies conducted in a drop tower [7] are numerically analyzed using a sphero-symmetric droplet combustion DNM that considers full multistage detailed chemical kinetics, multi-component transport, and spectral radiative interactions. *A priori* predictions are found to compare favorably with all of the experimentally measured droplet and flame diameter evolution histories, and diffusive extinction results. The simulations are also used to further elucidate the effects of a range of PRF fuel blend ratios on *CF* droplet burning behavior. Additional numerical simulations also suggest that *CF* droplet burning behaviors might be achievable for sub-millimeter PRF droplets with 50% *iso*-octane through replacement of small amounts of nitrogen inert by ozone.

2. Experimental setup and procedure

The large initial droplet sizes that have been conducive to promoting droplet burning behavior at standard atmospheric conditions can only be accessed in the Multi-user Droplet Combustion Apparatus (MDCA) of the "Combustion Integrated Rack" (CIR) on the ISS. The PRF droplets studied were “free-floated” to promote spherical symmetry during combustion. The experimental procedure is briefly discussed below. Further details are provided elsewhere [8,9].

Free floating droplets are deployed by rapidly retracting two opposed needles across which a liquid bridge is formed. Liquid is first dispensed through one of the needles and a liquid bridge is then formed by incrementally retracting the needles. The needles are then fully retracted to leave behind the test droplet with very low gas/droplet relative velocity. Combustion is then initiated by electrically energizing two Kanthal coils symmetrically positioned about the untethered droplet. The coils are subsequently retracted away from the droplet to allow the droplet to burn in an unobstructed ambience.

The diagnostics for the experiments consist of a High Bit-Depth Multispectral (HiBMs) camera (1 MP at 30 fps) with a backlight source and a color camera (0.3 MP at 30 fps) to record the droplet burning processes. Images are analyzed to obtain quantitative measurements of droplet and flame diameters as a function of time (t). Detailed methods for image analyses and measurements are described in previous publications [7,8,10]. Representative properties of *n*-heptane and *iso*-octane are given in Table 1.

3. Numerical modeling

The mathematical model employed in the current work is a transient, sphero-symmetric droplet combustion model featuring detailed gas phase kinetics, spectrally resolved radiative heat transfer and multi-component gas phase transport. Consistent with previous modeling efforts [12] that demonstrated “well mixed” conditions closely represent the enhancement of liquid phase transport due to internal motions within the liquid phase, the bi-component droplets are assumed to be initially homogenous employing a methodology discussed in [13]. Furthermore, the liquid mixture is considered to be ideal. Details of the base model and numerical methods have been reported previously in [14].

The present simulations incorporate a kinetic model for *n*-heptane and *iso*-octane blends

Table 1
Selected properties of *n*-heptane and *iso*-octane [11].

Property	*n*-C_7H_{16}	*iso*-C_8H_{18}
Molecular weight, M_w (g/mol)	100.20	114.23
H/C atomic ratio	2.28	2.25
Boiling point, T_b (K)	372.0	372.4
Flash point, T_f (K)	269	261
Density*, ρ_l (kg/m^3)	679.5	692.0
Specific heat*, $c_{p,l}$ (kJ/kg K)	2.242	2.123
Heat of vaporization, $\Delta H_v@T_b$ (kJ/mol)	31.77	30.79
Heat of combustion, ΔH_c (kJ/mol)	4849.2	5463.0

* Values of density and specific heat are @ 298 K.

consisting of 298 species and 1916 reactions. It consists of a reduced *n*-heptane kinetic model [3] with an embedded *iso*-octane subset taken from Mehl et al. [15]. The DNM also includes an appended PAH sub-mechanism taken from Raj et al. [16] to consider the potential for the formation of high molecular weight species (i.e. soot precursors in the gas phase). Finally ozone reaction kinetics from Halter et al. [17] and Ombrello et al. [18] were appended to the PRF model only for numerical computations involving ozone. The kinetic model is sufficiently complete to resolve low temperature, NTC, hot ignition, and high temperature kinetic behaviors.

The complete set of coupled partial differential and algebraic equations are discretized first in space and then integrated in an automated fashion as a set of coupled ordinary differential-algebraic equations in time. Spatial discretization is performed according to a node-centered finite volume scheme with second order accuracy. The gas–liquid interface demarcates the volume boundaries where an inner zone represents the condensed phase liquid fuel and an outer zone represents the gas phase ambient and the far field (typically two hundred times the initial droplet diameter). Dirichlet conditions for fixed ambient composition and temperature are imposed on the far-field. The innermost liquid node is centered at the origin, providing the required no-flux condition. To avoid oscillatory solutions, the discretized mass flux is represented on cell interfaces and not cell centers in the manner traditionally referred to as a "staggered grid". Numerical integration of the final set of discretized equations is performed using a backward difference formula with a variable order of up to fifth order and a variable time step utilizing a fully implicit multipoint interpolation, which is appropriate for the large range of time scales and stability constraints imposed by chemically reacting systems when combined with automatic time-step variation. The results reported in this work are for a grid configuration having 50 and 250 points in the liquid and gas phase respectively for the larger droplets and a 30, 120 point grid arrangement for the sub-millimeter sizes. An interface-tracking adaptive grid methodology is employed where a re-meshing is performed at every time step. Grid independent solutions were confirmed for the aforementioned grid configurations.

4. Results and discussion

First, we discuss simulations for a PRF50 droplet of initial diameter, $D_o \approx 3.51$ mm burning in atmospheric pressure air (simulating experiment FLEX 781). Simulations and data are also presented for a previously reported PRF50 drop tower experiment [7] using a sub-millimeter diameter droplet ($D_o = 0.52$ mm) and identical composition and atmospheric conditions.

Figure 1a compares predicted and measured droplet and flame diameters for both droplet sizes, while Fig. 1b presents the predicted evolution of the burning rate (K, with peak temperature shown in the inset). The measured droplet and flame diameter temporal evolutions are obtained from analyzing individual video images. The measurement uncertainties arise from identifying the boundary thickness of the droplet and flame, which consist of 3 and 5 pixels, respectively. In terms of pixel counts, measured droplet diameter range from ~88 to 124 pixels, resulting in an uncertainty of ± 2.4–3.4% for the droplet diameter measurements. The flame diameter measured in this study comprised ~62–208 pixels, ensuing in the uncertainty of a flame diameter ranging from ± 2.4 to 8.1%. Details on the uncertainty quantification are provided in Dietrich [9]. The measured evolution of burning rates as well as droplet and flame diameter are all well predicted, without parameter adjustments, giving credence to the selected combustion kinetics and property data inputs to the numerical simulation.

The results for $D_o = 3.51$ mm in Fig. 1a exhibit the characteristic features of *CF* droplet burning: an initial transient hot flame (radiative) extinction at $t/D_o^2 \approx 0.51$ s/mm^2 (at which time the video images cease to show a visible droplet flame) after which the burning rate (Fig. 1b) is significantly reduced and the flame standoff ratio (FSR, D_f/D) drops (the flame temperature shown in Fig. 1b was defined as the location of the peak

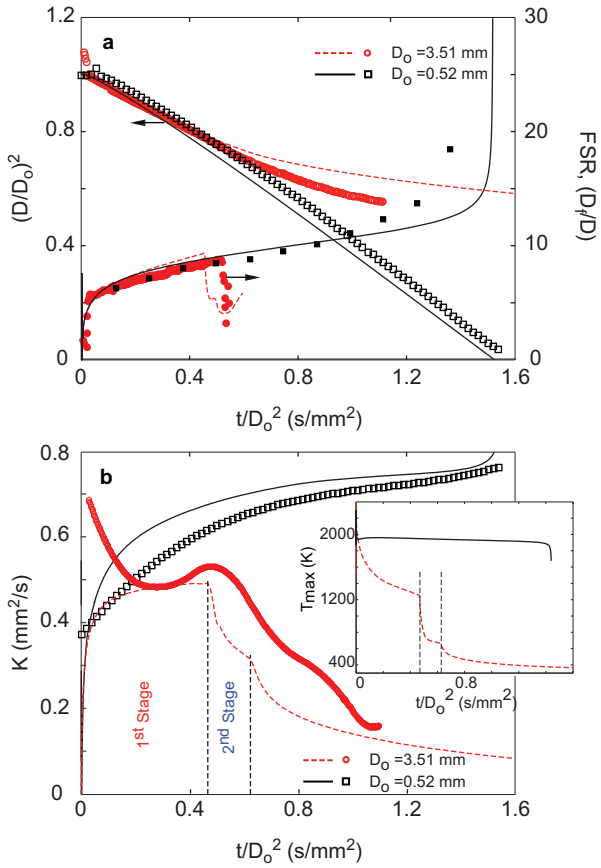

Fig. 1. Evolution of (a) droplet and flame diameter and (b) burning rate and peak temperature (inset) during the combustion of a droplet having an *n*-heptane + *iso*-octane blend. (O_2/N_2 0.21/0.79, blend of 50-50 by volume,1 atm). Symbols and lines represent experimental measurements and model predictions, respectively. Combustion characteristics of both $D_o = 3.51$ mm and $D_o = 0.52$ mm droplets are shown. The data for the sub-millimeter droplet comes from Liu and Avedisian [7].

gas temperature). The predicted flame temperature after radiative interesting is quite low – ~700 K – compared to the early hot-flame burning regime where it is ~2000 K (Fig. 1b). This second stage *CF* droplet burning occurs for a relatively shorter duration. In contrast to these results for a large PRF50 droplet, both the small droplet data ($D_o = 0.52$ mm) and predictions exhibit only hot flame combustion characteristics, with no transition to *CF* droplet burning behavior as shown in Fig. 1.

For the large diameter case, the predicted burning times for the first (hot) and second (*CF*) stages are $t_{b1\_model} = \sim 6.20$ s and $t_{b2\_model} = \sim 3.18$ s, respectively. For comparison, the experimental values are $t_{b1\_expt} = \sim 6.54$ s, $t_{b2\_expt} = \sim 3.33$ s. The predicted average burning rates and the extinction diameters for the two burning regimes are $K_{1\_avg\_model} = \sim 0.478$ mm^2/s, $D_{ext1\_model} = \sim 3.10$ mm and $K_{2\ avg\_model} = \sim 0.355$ mm^2/s, $D_{ext2\_model} = \sim 2.89$ mm. The comparable experimental values are $K_{1\ avg\_expt} = \sim 0.512$ mm^2/s and $K_{2\ avg\_expt} = \sim 0.382$ mm^2/s for the average burning rate, and $D_{ext1\_expt} = \sim 3.00$ mm and $D_{ext2\_expt} = \sim 2.78$ mm for the extinction diameters. The experimental burning rate constant is obtained from a linear fit of the experimental data during the period where the regression behavior is visually linear after any transients appear to decay. The simulation results were time averaged between $0.10 \le t_b \le 0.90$, (t_b is the burn time of the individual stages i.e. hot flame or *CF*) to determine the predicted burning rate constant. The differences of predicted and measured burning rates likely arise from experimental aberrations induced by the ignition event and other asymmetric behaviors, the way the ignition source is prescribed (i.e. energy deposition and duration) in the simulations [19], and the fact that the experimental burning rates are based on differentiating somewhat noisy data. The most prominent source for error in the experimental burning rate values arises from applying a

polynomial fit to the droplet diameter regression data so that a differentiation operation can be performed to obtain the K value. The uncertainty in such a process of evaluating burning rates could be as high as 5% depending on the noise of the data and choice of different polynomial fits [20].

As shown in Fig. 1b, the sub-millimeter PRF50 droplet data display a single-stage high temperature burn with an average predicted peak flame temperature of ~1920 K. Though the kinetics of the mixture components are distinctly different in the low, NTC, and hot ignition regimes, (i.e. significant low temperature, NTC kinetic activity for *n*-heptane, but low activities for *iso*-octane at atmospheric pressure[1]), their high temperature kinetic behaviors are qualitatively similar. Along with the similar component properties (e.g., boiling points and heats of vaporization, H/C ratio, see Table 1) high temperature droplet burning properties are a weak function of PRF mixture fraction. Moreover, neither the measurements nor the predictions show evidence of preferential vaporization phenomena affecting either burning rates or flame standoff ratios [7].

Interestingly, the predicted and experimental FSR's (Fig. 1a) for the large droplet during the high temperature burning stage agree with those for the smaller droplet despite the large difference in initial droplet diameter (factor of 6.75). At large extents of burning for the smaller droplet case, FSR predictions diverge from the experimental data, increasing more rapidly with extent of reaction. Continuous increases in FSR are expected as a result of thermal and diffusive buffering of the far field to heat loss and oxygen supply, and the significant increase in FSR noted experimentally forecasts considerably larger fuel vapor accumulation than the predictions. With capabilities of the DNM to predict experimental features of the PRF50 droplets established, we turn to using the model to understand certain features of the droplet burning process.

The temporal evolution of predicted peak concentrations of some dominant species for $D_o = 3.51$ mm are depicted in Fig. 2. The temporal evolution of peak species concentrations sharply delineates the two distinct combustion stages – high temperature and low temperature burning. During high temperature burning, the major combustion products are CO_2 and H_2O (Fig. 2a). The transition to low temperature burning coincides with a significant decrease in the rate of production of CO_2 and an accompanying accumulation for its precursor species, CO. The inhibitive nature of *iso*-octane to the low temperature kinetic behavior of pure *n*-heptane suppresses the second stage

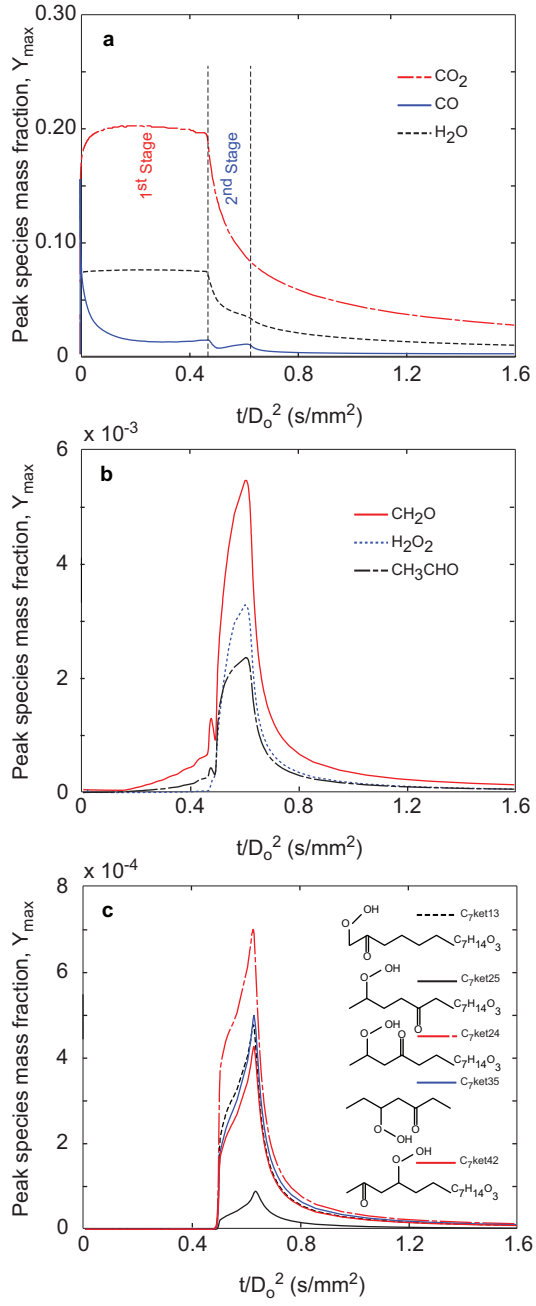

Fig. 2. Simulated temporal evolution of maximum species concentration (a) CO_2, CO and H_2O (b) H_2O_2, CH_2O and CH_3CHO and (c) $C_7H_{14}O_3$ during the combustion of a droplet having an *n*-heptane + *iso*-octane blend. ($D_o = 3.51$ mm, O_2/N_2 0.21/0.79, 50-50 *n*-C_7H_{16} *iso*-$C_8H_{1/8}$ blends,1 atm).

[1] It is well known that *iso*-octane shows low temperature reactivity only at very high pressures [21].

burn time associated with *CF* droplet burning. Despite the short duration in the current large droplet experiment, the second stage burn shows all the distinct characteristics of low temperature kinetics; higher concentrations of H_2O_2, CH_2O, CH_3CHO (Fig. 2b) and $C_7H_{14}O_3$ (Fig. 2c).

A flux analysis indicates that the bulk of *n*-heptane consumption during *CF* droplet burning occurs through H abstraction reactions by OH radicals and, to a much lesser extent, by HO_2 radicals. Beta scission reactions of the resulting *n*-heptyl radicals typically dominant in high temperature combustion cease to be significant, and are instead consumed by addition reactions with O_2 to form $\dot{R}O_2$radicals. Alkyl peroxy radical isomerization follows, forming QOOH. The QOOH formed is consumed through two competing pathways: (1) formation of $QOOHO_2$ through O_2 addition; and (2) decomposition to alkenes, carbonyl, QO, OH and HO_2. During the second stage combustion of the droplet, a major portion of the QOOH undergoes cyclization of the diradical to form cyclic ethers (QO). The decomposition of QOOH results only in radical propagation. $QOOHO_2$ surviving the decomposition reaction participates in the isomerization processes to form ketohydroperoxides ($C_7H_{14}O_3$). As for the *iso*-octane, it undergoes H abstracts predominantly by OH radical and also by H and HO_2 radical forming the *iso*-octyl radical. The *iso*-octyl decomposes to produce *iso*-butene (C_4H_8), propene (C_3H_6) and some C_7 alkenes. As *CF* droplet burning extinguishes, the droplet is still composed of ample quantities of both *n*-heptane and *iso*-octane.

Since the blend ratio dictates the duration and hence the presence of *CF* droplet burning, simulations were carried out to identify the role of blend ratio on multiphase combustion for the FLEX experimental conditions. From Fig. 3, it is evident that increasing the mole fraction of *iso*-octane decreases the hot flame burning phase prior to radiative extinction, accelerates the onset, decreases the duration of any subsequent *CF* droplet burning phase, and increases the final extinction diameter.

Figure 3a shows the evolution of predicted normalized droplet diameter for the indicated mixture fraction. The burning rate is independent of composition prior to the onset of radiative extinction, which is also consistent with reported data for small droplets [7]. At a 25% *iso*-octane volume fraction, the *CF* droplet burning rate is observed to decrease significantly. When the *iso*-octane fraction is increased to 50% the *CF* droplet burning time becomes very short before extinction occurs. Beyond a 50% blend ratio *CF* droplet burning is not evident in the simulations and the droplet undergoes a classical radiative extinction process to yield very large extinction diameters. The burning characteristics for *n*-heptane droplets containing 75 or 100% *iso*-octane are almost identical as shown in Figs. 3b and c.

Despite the variation of the onset time and duration of the *CF* droplet burning shown in Fig. 3c, the *CF* droplet burning flame temperatures for all the cases are predicted to be ~700 K, with a slight decrease of about 25 K as the *iso*-octane fraction is increased. Additionally, the temperature at which a transition to the second stage *CF* regime takes place increases with increasing *iso*-octane fraction. For pure *n*-heptane the transition takes place at ~1225 K, for PRF50 ~1270 K and for pure *iso*-octane radiative extinction occurs at ~1310 K – a significant increase in the temperature at which the system undergoes a possible transition. Furthermore, as the *iso*-octane fraction is increased the flame diameter at transition is slightly larger. A combined effect is enhanced radiative heat loss from the flame contributing to a shorter hot flame burn. The above results further establish the utility of the DNM for predicting and understanding *CF* droplet burning dynamics as influenced by initial diameter and PRF mixture fraction.

It is instructive to also simulate the influence of PRF mixture composition on shock tube ignition delay times under atmospheric pressure and stoichiometric conditions. The inset to Fig. 3c shows that as the *iso*-octane mixture fraction is increased the low temperature and NTC ignition delay characteristics between 600 and 825 K diminish and disappear entirely for pure *iso*-octane. The reduction in low and NTC kinetic behaviors with increasing PRF values is consistent with expectations from shock tube ignition delay data [21,22].

Affecting the balance of heat addition and loss during the initiation of droplet burning has been noted above as a key element in establishing *CF* droplet burning phenomena for fuel mixtures having multistage kinetic behaviors. In the above circumstances, *CF* droplet burning could only be established by initiating processes that result in a first stage hot flame combustion that was subsequently terminated by radiative extinction. If means could be achieved to limit the amount of initiation energy to that is sufficient to transition only to low temperature burning, perhaps hot flame initiation and a requirement for radiative extinction might be avoided. For the relatively volatile PRF components, droplets at room temperature already generate a significant volume of stratified flammable vapor/oxidizer mixture over the droplet surface through quasi-steady evaporation. Ignition energy delivered by sparks, arcs, or hot wire igniters to initiate reaction within the layer typically result in inflammation of the entire mixture. The accompanying chemical heat release drives the system toward hot flame behavior that can only be terminated by radiative heat losses. We ask what if only very small amounts of energy could be deposited over a longer time to drive initiation of low

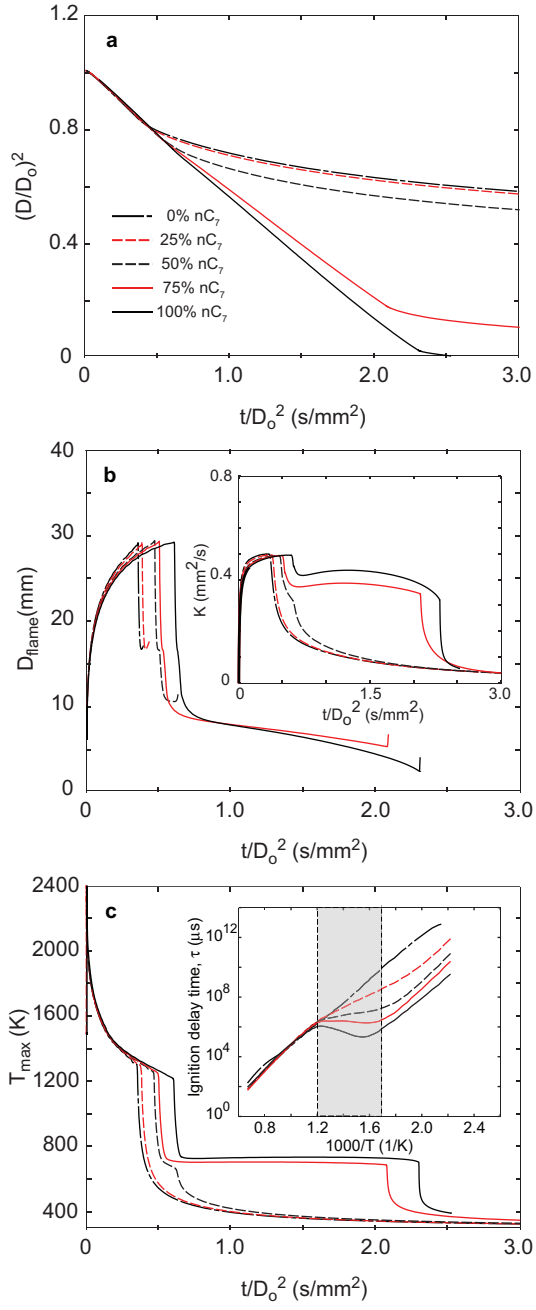

Fig. 3. Predicted evolution of (a) droplet diameter, (b) flame diameter and (c) peak temperature for varying fuel blends ($D_o = 3.51$ mm, O_2/N_2 0.21/0.79,1 atm). The burning rate evolution is provided as an inset in "b". Predicted shock tube ignition delay times for different primary reference fuel blends at atmospheric pressure and stoichiometric conditions are shown as an inset in "c".

temperature reaction of the surrounding flammable layer?

Recent computational efforts [23,24] suggest the possibility of directly inducing sustained *CF* droplet burning of even sub-millimeter *n*-heptane droplets by replacing small amounts of the nitrogen diluent with ozone (O_3). The ozone sensitizes the initiation of low temperature oxidative

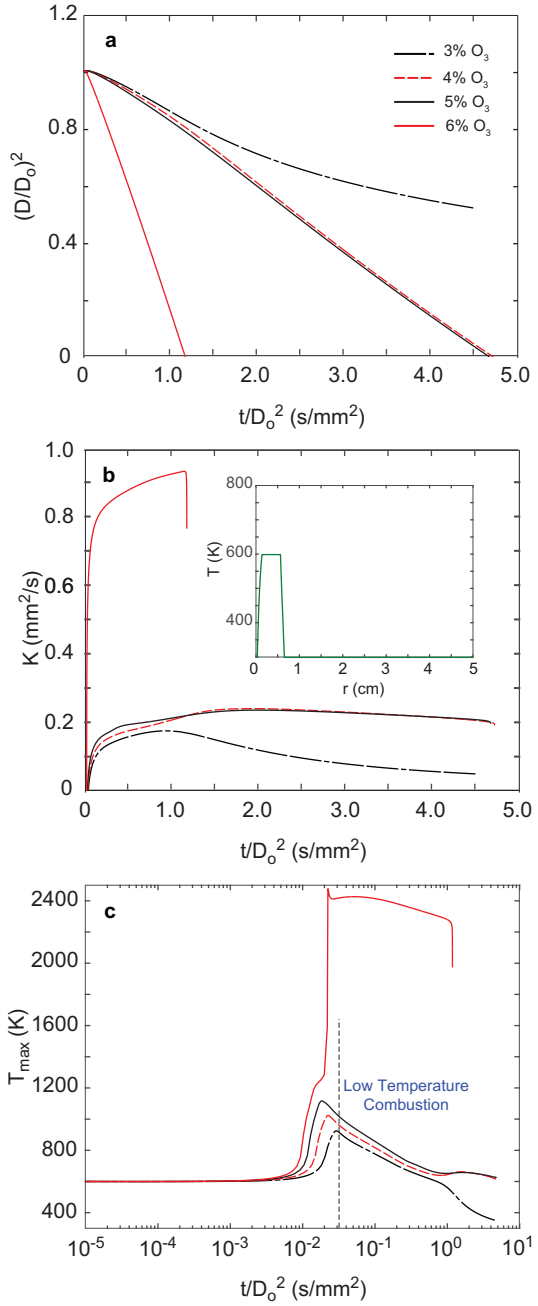

Fig. 4. Predicted combustion characteristics the evolution of (a) droplet diameter, (b) burning rate and (c) peak temperature a sub-millimeter blended *n*-heptane *iso*-octane (50-50 by volume) droplet in the presence of low ozone concentration ($D_o = 0.52$ mm, $O_2/O_3/N_2$ 0.21, prescribed ozone concentration and balance nitrogen at 1 atm).

chemistry, which through the accompanying heat release drives the system into sustained *CF* droplet burning (dominated by NTC kinetic behavior). Here, we apply the same approach to investigate numerically the potential of driving even sub-millimeter initial droplets of PRF50 directly into the *CF* droplet burning mode.

The combustion characteristics of a $D_o = 0.52$ mm *n*-heptane/*iso*-octane mixture droplet in atmospheric pressure air with small ozone mole

fractions systematically exchanged for nitrogen were simulated. To initiate the computations, a peak temperature of 600 K was prescribed as the initial ignition source (Fig. 4b inset). Figure 4 shows the predicted droplet diameter (4a), burning rate constant (4b) and (4c) peak gas temperature histories.

For trace ozone concentrations ($X_{O3} = 2\%$, not shown), the droplet experiences a low temperature initiation, does not transition to sustained *CF* burning, and extinguishes at very large diameters. As the ozone concentration is increased (e.g., $X_{O3} = 4\%$), sustained *CF* droplet burning is established directly (without transition through hot flame dynamics) as evidenced by low peak gas temperatures (in Fig. 4c). Interestingly for $X_{O3} = 3\%$, a *CF* burn to completion is not observed. The flame undergoes a diffusive extinction at a finite diameter, which in this case is caused by limitation of kinetic rates as the system transitions from NTC to low temperature kinetic regimes, i.e. an extinction governed by *diffusive-kinetic* coupling.

Increasing the ozone concentration further, leads to more rapid inception of first stage autoignition. Similar to the notion of a "threshold minimum ozone concentration" for persistent quasi-steady *CF* droplet burning, there also exists an upper limit of the ozone level above which only a transition to high temperature combustion is observed. For $X_{O3} = 6\%$, the droplet burning history shown in Fig. 4a corresponds to peak flame temperatures (Fig. 4c) indicative of hot flame combustion, but droplets are sufficiently small to preclude radiative extinction. Thus, there exists a relatively narrow range of ozone concentrations for which quasi-steady *CF* droplet burning behavior are developed directly from, and sustained after, the application of ignition energy to the droplet.

The role of ozone differs depending on the fuel vapor pressure (volatility) [25]. Ozone decomposes readily at reasonably low temperatures, yielding O radicals resulting in a net gain of O in the radical pool [26,27]. These radicals then, in a closed-loop feedback fashion, take part in further decomposing the available ozone. For a fuel that has higher vapor pressure e.g., *n*-heptane, these O radicals then directly take part in reacting with the fuel vapor and the exothermicity of ozone decomposition reactions have a secondary effect. However for a low vapor pressure fuel e.g., decane, the initial radical pool of O does not have significant fuel vapor present in the system with which to react. As a result they participate in further ozone decomposition reactions. The exothermic reactions associated with ozone decomposition give rise to time-varying temperatures during the early reaction stage (initial temperature ramp up) which drives the system to provide sufficient fuel vapor to reach the critical fuel vapor and oxidizer critical limit. At higher ozone concentrations, the O radical pool reaches a threshold condition resulting in a thermal runaway to a high temperature burn as shown in Figs. 4a and c. Predictions exhibit no such scenario for PRF mixtures with larger fractions of *iso*-octane.

5. Summary

New experimental data for large diameter PRF50 droplet combustion in atmospheric pressure air have been reported that show the presence of *CF* droplet burning. Simulations were conducted using a transient sphero-symmetric model with detailed chemistry that included both high temperature and low temperature kinetics. The *a priori* predictions were found to be in good quantitative agreement with the experimental measurements. The simulations indicate that the liquid fraction of *iso*-octane in PRF mixtures dictates the two-stage burning behavior. Unlike the large droplets which undergo multistage hot/*CF* droplet burning and radiative extinction, sub-millimeter PRF droplets produce only a high temperature burning stage with no evidence of preferential vaporization effects of the PRF components. Simulations were also used to assess a strategy for producing a *CF* droplet burning regime for sub-millimeter PRF droplets by incorporating small quantities of ozone in the surrounding air. Direct transition of *CF* droplet burning for sub-millimeter PRF50 droplets at atmospheric pressure is predicted for a narrow range of inert nitrogen replacement by 2–6 % ozone. The prospect that properly formulated, small diameter, ground-based experiments may yield *CF* droplet burning phenomena remains as future work.

Acknowledgments

This study was supported by the National Aeronautics and Space Administration (NASA) through grant numbers NNX14AG461A (TF), NNX08AI51G (YX and CTA) and NNX09AW19A (FLD). Special thanks go to Daniel Dietrich, Vedha Nayagam and Michael Hicks of NASA for their interest in our work and their help with the ISS experiments. The assistance of Meilin Dong, Hee Dae Tak and Do-Hyun Chung of Cornell with the ISS experiments and analysis of some of the video images that resulted is gratefully acknowledged. Conversations with Yu-Cheng Liu of Tsinghua University related to the experimental work are appreciated.

References

[1] V. Nayagam, D. Dietrich, M. Hicks, F. Williams, Combust. Flame 165 (5) (2015) 2149–2147.
[2] V. Nayagam, D.L. Dietrich, P. Ferkul, M.C. Hicks, F.A. Williams, *Combust. Flame* 159 (2012) 3583–3588.

[3] T. Farouk, F. Dryer, *Combust. Flame* 161 (2014) 565–581.
[4] Y. Liu, Y. Xu, M. Hicks, C.T. Avedisian, *Combust. Flame* 171 (2016) 27–41.
[5] P.S. Veloo, S. Jahangirian, F.L. Dryer, in: An experimental and kinetic modeling study of the two stage autoignition kinetic behavior of C_7, C_{10}, C_{12}, and C_{14} n-alkanes. Spring Technical Meeting of the Central States Section of the Combustion Institute, Dayton, Ohio, April 22–24, 2012.
[6] T. Farouk, M. Hicks, F. Dryer, *Proc. Combust. Inst.* 35 (2015) 1701–1708.
[7] Y. Liu, C.T. Avedisian, *Combust. Flame* 159 (2012) 770–783.
[8] D. Dietrich, V. Nayagam, M. Hicks, et al., *Microgravity Sci. Technol.* 26 (2014) 65–76.
[9] D. Dietrich, *Technical Publication NASA/TP-2013-216046 NASA*, Glenn Research Center, Cleveland OH 44135, USA, 2013 December 2013.
[10] C. Dembia, Y.C. Liu, C.T. Avedisian, *Image Anal. Stereol.* 31 (2012) 137–148.
[11] D.R. Lide, W.M. Haynes, *CRC Handbook of Chemistry and Physics*, 90th ed, CRC Press, Boca Raton, FL, 2010.
[12] A. Kazakov, J. Conley, F.L. Dryer, *Combust. Flame* 134 (2003) 301–314.
[13] A.J. Marchese, F.L. Dryer, *Combust. Flame* 105 (1996) 104–122.
[14] T. Farouk, F.L. Dryer, *Combust. Theory Model.* 15 (4) (2011) 487–515.
[15] M. Mehl, W. Pitz, C. Westbrook, Curran, *Proc. Combust. Inst.* 33 (2011) 193–200.
[16] A. Raj, I.D.C. Prada, A.A. Amer, S.H. Chung, *Combust. Flame* 159 (2012) 500–515.
[17] F. Halter, P. Higelin, P. Dagaut, *Energy Fuels* 25 (7) (2011) 2909–2916.
[18] T. Ombrello, S.H. Won, Y. Ju, S. Williams, *Combust. Flame* 157 (10) (2010) 1906–1915.
[19] T. Farouk, Y.C. Liu, A.J. Savas, C.T. Avedisian, F.L. Dryer, *Proc. Combust. Inst.* 34 (1) (2013) 1609–1616.
[20] Y.C. Liu, A.J. Savas, C.T. Avedisian, *Energy Fuels* 26 (9) (2012) 5740–5749.
[21] D. Davidson, S. Ranganath, K. Lam, M. Liaw, Z. Hong, R. Hanson, *J. Propuls. Power* 26 (2) (2010) 280–287.
[22] H. Shen, J. Steinberg, J. Vanderover, M. Oehlschlaeger, *Energy Fuels* 23 (2009) 2482–2489.
[23] F. Alam, F. Dryer, T. Farouk, in: Ozone assisted "Cool Flame" combustion of sub-millimeter n-heptane droplets at atmospheric and higher pressure. 9th US National Combustion Meeting, Cincinnati, Ohio, May 17–20, 2015.
[24] T. Farouk, D. Dietrich, F. Alam, F. Dryer, *Proc. Combust. Inst.* (2016), doi:10.1016/j.proci.2016.07.015.
[25] F. Alam, S. Won, F. Dryer, T. Farouk, *Combust. Flame* (2016) In Review.
[26] T. Ombrello, S.H. Won, Y. Ju, S. Williams, *Combust. Flame* 157 (2010) 1906–1915.
[27] G.D. Smekhov, L.B. Ibraguimova, S.P. Karkach, O.V. Skrebkov, O.P. Shatalov, *High Temp.* 45 (2007) 395–407.